Pramana – J. Phys. (2019) 93:15
https://doi.org/10.1007/s12043-019-1778-3

Design of a spiral inflector and transverse beam matching for K130 cyclotron at the Variable Energy Cyclotron Centre

A GOSWAMI[1,2,*], ATANU DUTTA[1] and SANTANU PAUL[1,2]

[1]Variable Energy Cyclotron Centre, 1/AF, Bidhan Nagar, Kolkata 700 064, India
[2]Homi Bhabha National Institute, Anushakti Nagar, Mumbai 400 094, India
*Corresponding author. E-mail: animesh@vecc.gov.in

MS received 13 September 2018; revised 28 December 2018; accepted 21 January 2019;
published online 13 May 2019

Abstract. This paper describes the design of a spiral inflector for inflecting heavy ion beams into the existing central region of the K = 130 Variable Energy Cyclotron at Kolkata. Simulation results of transverse beam dynamics through the spiral inflector and the effect of the fringe field on beam phase ellipses at its exit have been discussed in the absence of space charge effect. We have also made an effort to minimise the effect of inflector fringe field by properly adjusting the inflector voltage. The proper matching conditions in the central region have been obtained by optimising the system parameters of the existing axial injection line of K130 cyclotron. The tracking of particles that belong to the boundary of the optimised phase ellipses at the matching point has also been carried out in the computed electric and magnetic fields in the central region. Simulation results confirm that the optimised beam condition reduces beam losses for further acceleration in the cyclotron.

Keywords. Spiral inflector; fringe field effect; beam dynamics; transverse beam matching; central region; particle tracking.

PACS Nos 29.27.Bd; 41.85.Ja; 41.85.−p

1. Introduction

The variable energy cyclotron (VEC) with K = 130 at Kolkata is presently accelerating different types of light–heavy ion beams for doing research in basic nuclear physics, radiochemistry, materials science and many other related fields [1–4]. The K130 cyclotron has a water-cooled magnet with a pole diameter of 224 cm, weighing 262 tons [5–7]. It is a three-sector cyclotron with a maximum spiral angle of approximately 55° and a maximum average magnetic field of about 17 kG. The main magnet and 17 trim coils provide isochronous magnetic field for different ion species. The radio frequency system consists of 180° Dee, presently operating at a frequency from 5.5 MHz to 10.5 MHz with a maximum voltage of about 65 kV. The 14.4 GHz electron cyclotron resonance (ECR) ion source produces a variety of ion species at an extraction voltage of ∼ 8 kV–10 kV. The beam from the ion source is first analysed and then axially injected into the central region of the cyclotron by using a gridded electrostatic mirror inflector [8–10]. The mirror inflector consists of a pair of planar electrodes which are positioned at an angle of 46.3° to the incoming ion beam. A wire grid is positioned parallel to and 5 mm above the face of the electrode. The grid is grounded and a DC voltage is applied to the other electrode.

Although it is easy to construct the mirror inflector, it requires almost the same voltage as the injection voltage (∼10 kV) for the inflection of ions. Another disadvantage is that the grid wires have a limited lifetime as these are exposed to beams over a long period. Therefore, it becomes necessary to replace the assembly at regular intervals, thus increasing the downtime during experiments. The grids also cause beam degradation and transmission loss. A spiral inflector [11–18], consisting of coaxial spirally twisted electrostatic deflection plates, is the most widely used inflection device employed to bend and match an axially injected beam with the median plane of a cyclotron because of its flexibility, large acceptance, relatively low voltage requirement for operation and almost 100% transmission efficiency [19,20].

For a given injection energy and central magnetic field, the shape and size of a spiral inflector mainly depend on two adjustable parameters, the height of the inflector and the tilt angle. The design of a spiral inflector

has been described in [12,14,18] and the feasibility study of using a spiral inflector in a K130 cyclotron is reported in ref. [15]. Pandit [15] has neglected the effect of a fringe field at the entrance and exit of the spiral inflector. Due to the low injection energy of the beam (∼10 keV), the dimension of the inflector is comparatively small (height ∼ 2 cm). For smaller height of the inflector, the fringe field at the entrance and exit plays an important role, and hence the design of the inflector becomes more complicated and challenging. In the present work, we have carried out a detailed design study of a spiral inflector for K130 cyclotron at Variable Energy Cyclotron Centre (VECC) and studied its beam optical properties by using the more realistic electric field map produced by the code RELAX3D [21].

Transverse beam matching in the central region of the cyclotron is important to achieve optimum performance of the cyclotron. For a fixed geometry of the inflector, the beam properties at its exit strongly depend on the two transverse phase planes of the beam at the entrance of the inflector [18]. The emittances and orientations of beam ellipses at the exit of the spiral inflector should be matched with the acceptance of the central region for further efficient acceleration of the cyclotron. Any mismatch in the injection causes the amplitude growth of the beam during the acceleration which finally results in the loss of the beam. Moreover, before entering into the central region of the cyclotron, the injected ion beam encounters a rising magnetic field in the axial hole of the magnet where it is strongly focussed. This must be taken into account while performing the beam matching with the acceptance of the central region. The goal of the present work is also to find out the optimised parameters of the beam line elements in the axial injection system for proper matching of the ion beam.

The paper is organised as follows. In §2, a brief description of the coordinate system used in this work and the design of the spiral inflector are outlined. The electric and magnetic field components, the theory of the central ion trajectory and the design optimisation of the spiral inflector are discussed in §2.1 and 2.2. In §2.3, the effect of the fringe field on the central orbit is presented. The method to find the inflector transfer matrix and transverse beam dynamics in the spiral inflector is analysed in §3. Section 4 briefly discusses the optimisation procedure used in the present work for transverse matching of the beam with the central region of the cyclotron. The results of simulation are also presented in §4. Finally, conclusions are drawn in §5.

2. Spiral inflector design

The K130 cyclotron operates over a wide range of beams including light ions from an internal PIG ion source. The accelerating electrodes in the central region are specially designed to accommodate the PIG ion source internally and the mirror inflector when beam is axially injected. The goal is then to find out a suitable geometry of the spiral inflector that will produce a well-centred beam with the present central region geometry so that the switching between these two types of injections can be done very quickly. However, this constraint puts a restriction on the maximum size of the spiral inflector, including housing because it has to fit within the existing accelerating electrodes in the central region consisting of Dee and Dummy Dee inserts whose function is to provide vertical focussing and to decrease the transit time in the central region.

In this section first we briefly outline the analytical formulations used for the design of the spiral inflector and then study the effect of the fringe field on the orbit properties of the central ray.

2.1 *Coordinate system and central ray*

In a spiral inflector, a particle moves under the action of both electric and magnetic fields. To study the motion of a particle in a spiral inflector, two coordinate systems are generally used [17,22]. We have used the right-handed Cartesian coordinate system (x, y, z) with its origin in the cyclotron axis in the median plane and the x- and y-axes are in the median plane. The z-axis is vertically opposite to the direction of the incoming ion and the magnetic field (B_z) is opposite to the z direction. The electric field is along the x direction at the entrance of the inflector. The second coordinate system is the optical coordinate system (u, h, v) which moves in space along with the central ion trajectory. Vector $\vec{v}$ is along the direction of the velocity of the beam, vector $\vec{h}$ is always parallel to the median plane (x–y plane) and vector $\vec{u} = \vec{h} \times \vec{v}$. It is parallel to the median plane at the entrance of the inflector, changes its direction as the beam advances and becomes perpendicular to the median plane at the exit of the inflector. A schematic diagram of both the coordinate systems is shown in figure 1a.

If $v_0 = \sqrt{\dot{x}^2 + \dot{y}^2 + \dot{z}^2}$ is the velocity of an ion on the central trajectory, then the unit vectors $\hat{u}$, $\hat{h}$ and $\hat{v}$ can be expressed in terms of $\hat{x}$, $\hat{y}$ and $\hat{z}$ as [13]

$$\hat{u} = -\frac{\dot{x}\dot{z}}{v_0\sqrt{v_0^2 - \dot{z}^2}}\hat{x} - \frac{\dot{y}\dot{z}}{v_0\sqrt{v_0^2 - \dot{y}^2}}\hat{y} + \frac{\sqrt{v_0^2 - \dot{z}^2}}{v_0}\hat{z}, \tag{1a}$$

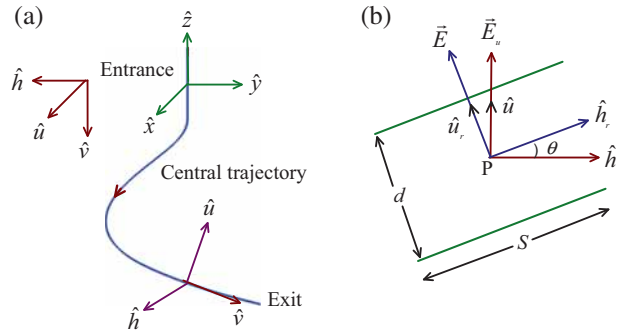

Figure 1. A schematic of (**a**) fixed right-handed Cartesian (x, y, z) with basis vectors $\hat{x}$, $\hat{y}$ and $\hat{z}$ and an optical (u, h, v) coordinate system with basis vectors $\hat{u}$, $\hat{h}$ and $\hat{v}$ and (**b**) spiral inflector geometry as viewed from a plane perpendicular to the central trajectory. Here d is the electrode spacing and S is the width of the electrodes.

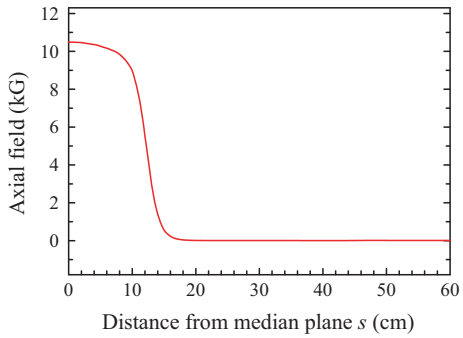

Figure 2. Variation of the magnetic field with distance s from the median plane along the cyclotron axis for 1056 A main magnet current. Data are obtained from 3D code.

$$\hat{h} = \frac{\dot{y}\hat{x} - \dot{x}\hat{y}}{\sqrt{v_0^2 - \dot{z}^2}}, \tag{1b}$$

$$\hat{v} = \frac{\dot{x}\hat{x} + \dot{y}\hat{y} + \dot{z}\hat{z}}{v_0}, \tag{1c}$$

where $\dot{x}$, $\dot{y}$ and $\dot{z}$ are the velocity components of the central ion along x, y and z-axis, respectively, and the dot denotes the differentiation with respect to time t.

Figure 1b shows the $u-h$ cross-sectional view along with a rotated optical coordinate system $(\hat{u}_\mathrm{r}, \hat{h}_\mathrm{r}, \hat{v})$ defined by rotating the vectors $\hat{u}$ and $\hat{h}$ about the vector $\hat{v}$ by an angle θ:

$$\hat{u}_\mathrm{r} = \cos\theta\cdot\hat{u} + \sin\theta\cdot\hat{h}, \quad \hat{h}_\mathrm{r} = -\sin\theta\cdot\hat{u} + \cos\theta\cdot\hat{h}. \tag{2}$$

To find the analytical electric field inside the spiral inflector, we have assumed that the u component of the electric field, E_u, is constant (E_0) at all points along the central trajectories and the v component of the electric field E_v is zero [13,19]. Using these assumptions and from figure 1b, the electric field in a tilted spiral inflector can be written as

$$\vec{E} = E_u\hat{u} + E_h\hat{h} = |\vec{E}|\cos(\theta)\hat{u} + |\vec{E}|\sin(\theta)\,\hat{h}, \tag{3}$$

where $|\vec{E}|$ is the electric field strength seen by the central ion trajectory and θ is the local tilt angle. From figure 1b we can write

$$|\vec{E}| = \frac{E_u}{\cos\theta} = \frac{E_0}{\cos\theta}. \tag{4}$$

Here E_0 is the magnitude of the electric field which is always constant and perpendicular to the direction of motion of the ion. For a given kinetic energy T of the beam, it decides the height parameter A of the spiral inflector, defined as $A = 2T/qE_0$. The local tilt angle θ used earlier is defined by

$$\tan\theta = k'\frac{A - z(s)}{A}, \tag{5}$$

where k' is a free parameter and it decides the maximum tilt angle $\theta_\mathrm{m} = \tan^{-1}k'$ at the exit of the inflector. Using eqs (1) and (4) in eq. (3) we can write the components of the electric field along the central trajectory in the spiral inflector as

$$E_x = E_0\left(-\frac{x'z'}{\sqrt{x'^2 + y'^2}} - \frac{y'}{\sqrt{x'^2 + y'^2}}\tan\theta\right), \tag{6a}$$

$$E_y = E_0\left(-\frac{y'z'}{\sqrt{x'^2 + y'^2}} + \frac{x'}{\sqrt{x'^2 + y'^2}}\tan\theta\right), \tag{6b}$$

$$E_z = E_0\sqrt{x'^2 + y'^2}, \tag{6c}$$

where prime denotes the derivative with respect to s.

In order to obtain the magnetic field in the K130 cyclotron, the magnet is simulated by using OPERA3D TOSCA solver [23]. The isochronous magnetic field is generated by using the main magnet coil and by adjusting 17 trim coils current independently. The current in the main magnet and trim coils is chosen to be very near to the present operational setting of the cyclotron. The variation of the computed magnetic field with distance s from the median plane along the cyclotron axis for 1056 A current is shown in figure 2. It is easy to see from figure 2 that the field is almost constant near the median plane and has a sharp gradient at the beginning of the central plug. As the height of the spiral inflector is very small, the magnetic field is taken to be constant over its length.

In the case of a constant magnetic field, i.e. $B_x = B_y = 0$ and $B_z = B_0$ and the electric field given in eq. (6), the components of the Lorentz force equation for a particle in the spiral inflector can be written as

$$x''(b) = A\big[\cos(2Kb)\cos b - k'\sin(2Kb)\sin b\big] - \frac{qA}{mv_0}y'(b)B_0, \tag{7a}$$

$$y''(b) = A\big[\sin(2Kb)\cos b + k'\cos(2Kb)\sin b\big] + \frac{qA}{mv_0}x'(b)B_0, \tag{7b}$$

$$z''(b) = A\sin b, \tag{7c}$$

where $b = (v_0 t/A) = (s/A)$ is the instantaneous angle of the velocity vector with the vertical axis. The shape parameter K in eq. (7) is defined as

$$K = \frac{A}{2R_\mathrm{m}} + \frac{k'}{2}. \tag{8}$$

Here $R_\mathrm{m} = p/qB_0$ is the magnetic radius of the ion with momentum p. Equation (7) can be solved analytically to yield the following parametric equations:

$$x(b) = \frac{A}{2}\left[\frac{2}{1-4K^2} + \frac{\cos[(2K-1)b]}{2K-1} - \frac{\cos[(2K+1)b]}{2K+1}\right], \tag{9a}$$

$$y(b) = -\frac{A}{2}\left[\frac{\sin[(2K+1)b]}{2K+1} - \frac{\sin[(2K-1)b]}{2K-1}\right], \tag{9b}$$

$$z(b) = A(1-\sin b), \quad 0 \le b \le \pi/2. \tag{9c}$$

Choosing a suitable value of A and k' one can easily find out the coordinates of the central ion trajectory from eq. (9). One of the important parameters required to be optimised in the design of the spiral inflector is the 'off-centre', i.e., the displacement of the centre of the trajectory from the vertical axis at the exit of the inflector. It is given by

$$\rho_\mathrm{c} = \sqrt{x_\mathrm{c}^2 + y_\mathrm{c}^2}, \tag{10}$$

where x_c and y_c are the coordinates of the centre of curvature at the exit of the inflector. One needs to optimise the off-centre parameter ρ_c at the exit of the inflector to meet the requirement of the proper orbit centring in the central region of the cyclotron. A proper choice of parameters A and k' plays an important role in the design of the spiral inflector. The height A of the inflector is limited by the space available in the central region. More tilt affects the beam emittance adversely [17], reduces the gap between the electrodes in the exit region and makes the fabrication of the inflector difficult.

Table 1. Central magnetic field for different ions.

Ion species	Magnetic field (B_0) (kG)
O^{5+}	11.50
O^{6+}	10.49
Ne^{6+}	11.73
Ne^{7+}	10.86
Ne^{8+}	10.16
Ar^{9+}	13.55

2.2 *Orbit calculations and design parameters*

In this subsection, we have presented the design results of the spiral inflector based on the theoretical model discussed above. The parameter $\chi = QB_0^2/A_\mathrm{m}$ is generally defined to describe the whole operating region of a cyclotron [15]. Here Q is the charge state, A_m is the mass number of the ion and B_0 is the central magnetic field. For VEC, for a range of B_0 from 5 kG to 17.1 kG and Q/A_m from 0.25 to 0.5, χ varies from 5 to 150. It is not possible to design a single spiral inflector which can cover the entire operating region and also fits into the space available in the central region without disturbing the existing accelerating electrode structure. We have chosen χ from 40 to 90 that includes a variety of light–heavy ions such as $O^{5+,6+}$, $Ne^{6+,7+,8+}$, Ar^{9+}, etc. We have designed a spiral inflector that can inflect these ions into the K130 cyclotron at VECC. In this case, the spiral inflector operates in the scaling mode which demands that the magnetic radius R_m of the ion must be constant:

$$R_\mathrm{m}(\mathrm{cm}) = \sqrt{20.88 A_\mathrm{m} V_\mathrm{ext}\,(\mathrm{kV})/Q B_0^2\,(\mathrm{kG})} = \mathrm{const.}, \tag{11}$$

where V_ext is the extraction voltage of the ion source in kV and B_0 is in kG. We have chosen the representative ion as O^{6+} with the central magnetic field $B_0 = 10.49$ kG and $V_\mathrm{ext} = 6.41$ kV. The value of R_m, in this case, is 1.8 cm. If we want to use the same spiral inflector for another kind of ion, the extraction voltage V_ext and the central field value B_0 for that kind of ion can be obtained by scaling according to eq. (11). For a given extraction voltage $V_\mathrm{ext} = 6.41$ kV, the required magnetic field B_0 for different ions are calculated by using eq. (11) and is listed in table 1.

The central trajectory in the spiral inflector is obtained by the analytical expression given in eq. (9) as well as by using the computer program CASINO [24] with a hard edge electric field. The design of an inflector is an iterative process. While designing an inflector, one needs to optimise the off-centre parameter at the exit

Table 2. Optimised parameters of the inflector.

Parameters	Values
Height (A)	1.6 cm
Tilt (k')	0.58
Electric field (E_0)	8.01 kV/cm
Aspect ratio (ξ)	1.5
Gap (d_0) entrance/exit	5 mm/4.3 mm
Position at exit (r, θ)	1.37 cm, 84.8°
Exit data (x_e, y_e)	(0.124, 1.364) cm

of the inflector to meet the requirement of the orbit centring of the beam in the central region. The height A and tilt k' are required to be adjusted properly to make the beam well centred. A suitable value of parameter A is chosen by considering a reasonable value of the electric field between the electrodes (<20 kV/cm) to avoid any sparking and the space available in the central region. As the height gets larger, the ion path becomes longer and the inflector requires more space in the central region. The tilt parameter k' is varied to produce the desired orbit centre at the inflector exit. For each set of A and k', we have calculated the off-centring and direction of the initial velocity vector of the central trajectory at the exit of the inflector and performed the orbit tracing using the central region code in the computed magnetic field of the K130 cyclotron. The gap between electrodes d_0 is chosen to be ∼5 mm to ensure the loss-free bending of the beam. The aspect ratio ξ, defined as the width of the electrode divided by the gap between the electrodes, is generally chosen to be 2 to avoid the effect of the fringe field. In the present design, ξ is taken to be 1.5 due to the space constraints in the central region. Important parameters of the inflector that has minimum off-centring and produces a well-centred orbit are listed in table 2.

The x–y and r–z projections of the central ion trajectory obtained from eq. (9) are shown in figure 3. The comparison of our result with the spiral inflector orbit code CASINO is also shown in the plot. We can see that the results are almost identical. The data of the central ion trajectory in the inflector obtained from the code CASINO has been used in the program INFLECTOR [25] to generate the shape of the electrodes and mesh points for RELAX3D [21] to compute the electric field distributions in the inflector.

Figure 4 shows the geometry of the spiral inflector without ground plates. The x–y projection of the shape of the two electrodes when $A = 1.6$ cm and $k' = 0.58$ is shown in figure 4a, whereas the schematic shape of the biased electrode surface of the spiral inflector is shown in figure 4b. It is evident from the plot that the beam can be injected and easily positioned in the central region with the existing Dee and Dummy Dee inserts. The grounded plates parallel to the inflector entrance and exit are placed 5 mm away from the inflector such that the opening of these plates coincides with the opening of the inflector at the entrance and the exit.

The orbit centring of the inflected beam was checked by using the central region code which solves the equations of motion in combined electric and magnetic fields using the fourth-order Runge–Kutta method. The coordinates and the direction of the velocity of the particle following the central trajectory were obtained at the matching point in the central region by CASINO and entered as an input to the central region code. The matching point is located at $x = -0.39$ cm and $y = 1.75$ cm in the median plane. All calculations of beam centring were performed for the O^{6+} ion when injection energy = 38.45 keV, Dee voltage = 48 kV, rf frequency = 6 MHz and harmonic number = 1. The gap width between the Dee insert and the Dummy Dee insert remains constant (0.9 cm) up to 5 cm radius and then gradually increases. The aperture of Dee insert and Dummy Dee insert changes from 1 cm at 2.1 cm radius to

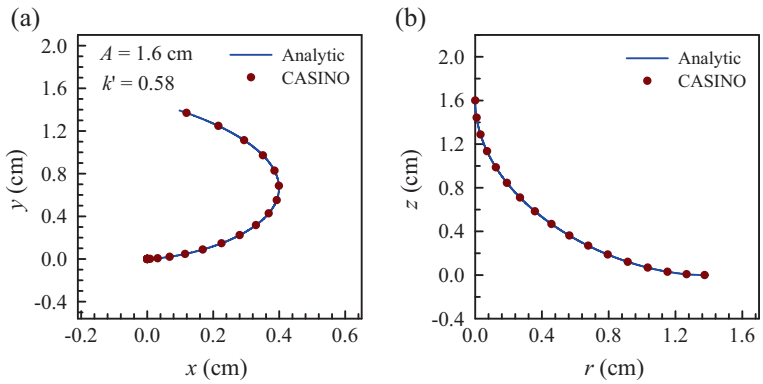

Figure 3. Central orbit for an analytic electric field distribution: (**a**) x–y projection and (**b**) r–z projection. The solid line and the filled circle represent the results obtained from analytical calculations and CASINO, respectively.

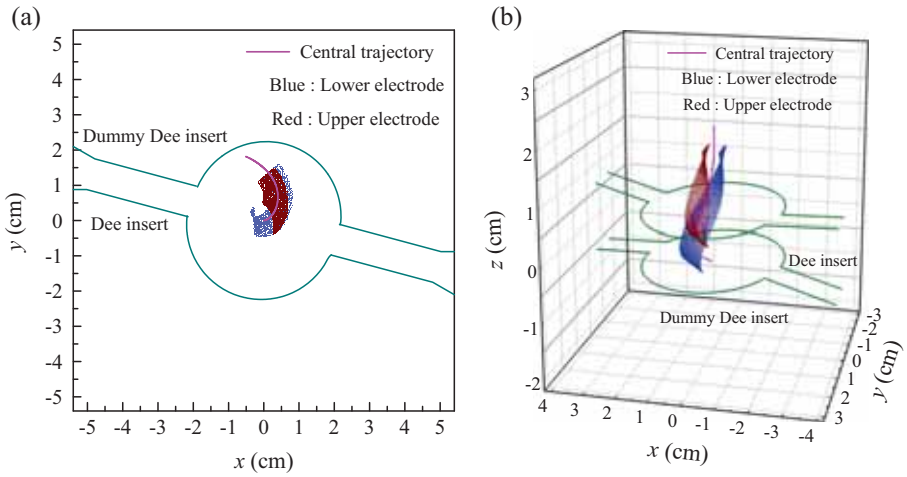

Figure 4. Schematic shape of the spiral inflector: (**a**) the x–y projection of the two-electrode shape and (**b**) biased electrode geometry. The central ion trajectory, Dee and Dummy Dee inserts are also shown in the plot.

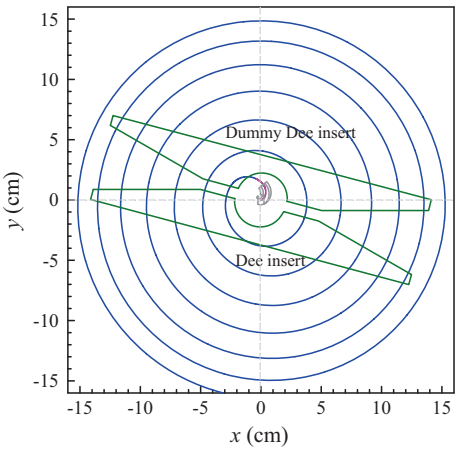

Figure 5. The projection of the inflector, location of the accelerating gaps in the central region and accelerated orbits of O^{6+} ions from 38.45 keV to 3 MeV. The pink solid line indicates the projection of the central ion trajectory of the inflector in the median plane.

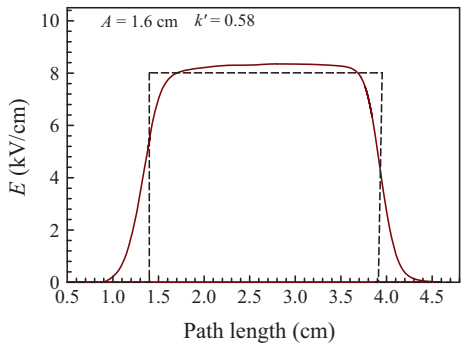

Figure 6. Comparison of the analytic (dotted line) and the computed (solid line) electric fields along the central ion trajectory in the spiral inflector. Data are obtained from RELAX3D.

1.4 cm at 5 cm radius and then gradually increases. The three-dimensional (3D) magnetic field distribution was obtained by OPERA. The magnetic field map $B(r, \theta, z)$ is stored in a polar grid with $\Delta r = 1$ cm, $\Delta\theta = 1^\circ$ and $\Delta z = 0.1$ mm. The 3D electric field distribution in the accelerating gaps has been numerically calculated using OPERA. For electrostatic simulation, part of the central region which extends up to almost 15 cm × 15 cm in the x and y directions (the x–y plane is the median plane) and ±4 cm in the z direction is meshed by tetrahedral meshes with a maximum size of 1 mm within the available aperture.

Figure 5 shows the horizontal cross-section in the central region, projection of the inflector, location of the Dee insert and Dummy Dee insert in the x–y plane and a few turns of the accelerated orbits of O^{6+} ions from 38.45 keV to 3 MeV. It is easy to see from figure 5 that the beam is well centred with the input condition provided by the spiral inflector at the matching point. The position of the orbit centre was also found to converge satisfactorily after a few turns.

2.3 *Fringe field effect*

The design of the spiral inflector has been done by assuming analytic electric field which has a hard edge at the entrance and exit of the inflector. A real inflector has a fringe field at its ends that makes the effective length of the inflector longer. Particularly, the effect of this fringe field is much significant for an inflector with a smaller height. Figure 6 shows the computed electric field strength on the central ion trajectory (u plane)

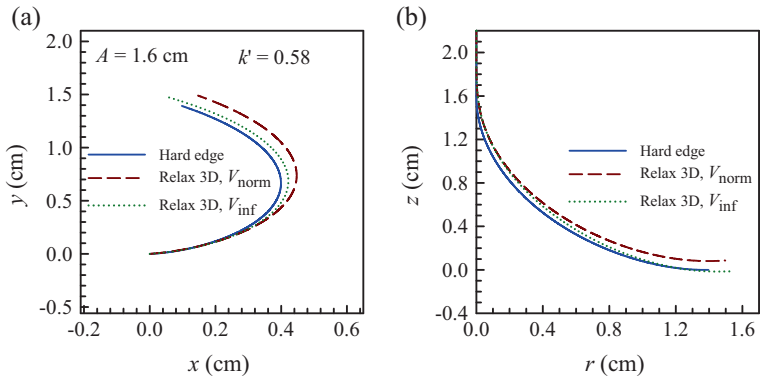

Figure 7. Comparison of the central orbit obtained from the hard edge electric field (solid line), a field from RELAX3D (dashed line) with V_{nom}, and a field from RELAX3D with a reduced voltage V_{inf} (dotted line): (**a**) x–y projection and (**b**) r–z projection.

and compares it with the analytical electric field (hard edge approximation) used for the initial design. It can be readily seen from figure 6 that the extension of the fringe field is significant at the entrance and the exit. This may be due to the comparatively smaller height A of the inflector in the present design.

Figure 7 compares the x–y and r–z projections of the central ion trajectory obtained by re-executing the program CASINO with both the electric fields obtained from the analytic hard edge approximation (the solid line) and from RELAX3D (the dashed line). It is easy to see from figure 7 that the fringe field causes the central trajectory of the inflector to deviate from the design orbit. In this case, the vertical momentum p_z of the ions is found to be non-zero at the median plane. We can compensate the fringe field of the inflector by decreasing the voltage between the inflector electrodes. The dotted line in figure 7 shows that the central ion trajectories are very close to the designed orbit when a 7.8% reduced voltage is applied. In this case, the condition $p_z = 0$ is satisfied in the median plane. Here V_{nom} is the biased voltage in the analytic inflector and V_{inf} is the reduced biased voltage to compensate for the fringe field effect. In the present case, $V_{\text{nom}} = \pm 2\,\text{kV}$ and $V_{\text{inf}} = \pm 1.85\,\text{kV}$.

3. Transverse beam dynamics

In order to study the beam dynamics through the spiral inflector we have used the linear transfer matrix technique. The space charge effect is not taken into account, as the extracted beam currents from the ECR ion source are of the order of a few tens of μA, which are at least an order of magnitude lower than the current reported to cause considerable space charge effects [17]. Paraxial ray equations through the spiral inflector [17,26] are linear. Therefore, any solution of these equations can be represented by the linear combinations of six linearly independent solutions. Let $\mathbf{x}(s_0) = (u, p_u, h, p_h, v, p_v)^{\text{T}}$ represents the coordinates of a paraxial ray at location s_0. At some other location s, the coordinates will be transformed according to the matrix equation $\boldsymbol{x}(s) = \mathbf{M}(s, s_0)\mathbf{x}(s_0)$, where $\mathbf{M}(s, s_0)$ is a 6×6 transfer matrix. An inflector with hard edge electric fields s_0 and s corresponds to the actual electrode start and end, respectively, whereas for a RELAX3D electric field, these correspond to the start and end location of the fringe field, respectively. To generate matrix $\mathbf{M}(s, s_0)$, we need to solve paraxial equations for six different initial conditions. These equations cannot be solved analytically [27]. Hence, a numerical integration method is needed to get the coordinates of the paraxial ray trajectory. This is done using the code CASINO.

To obtain the inflector transfer matrix, the five linearly independent paraxial rays are tracked through the spiral inflector using the CASINO code. As an initial condition for each of the rays, a displacement in one of the five coordinates u, h, p_u, p_h and p_v, is chosen with all other coordinates set to 0. We have not taken an initial v displacement because it produces a constant v displacement along the entire length of the trajectory. We tracked two displaced rays that have the same magnitude of displacement but are of opposite signs to reduce the nonlinearities present in the orbits calculated with CASINO. The output coordinates are then averaged to remove the remaining second-order term. We have taken the position displacement as 0.01 cm and momentum displacement as 0.001 rad. It is to be noted here that the initial conditions for forming the matrix element should be canonical so that matrix $\mathbf{M}$ should be a symplectic one. As the inflector is put in the axial magnetic field B_0 of the cyclotron, the variable $\mathbf{x}(s_0)$ is no longer canonical at the inflector entrance. To make the variables canonical, we need to modify them as

$$p_u^C = p_u + \frac{h}{2R_{\text{m}}}, \quad p_h^C = p_h - \frac{u}{2R_{\text{m}}}, \tag{12}$$

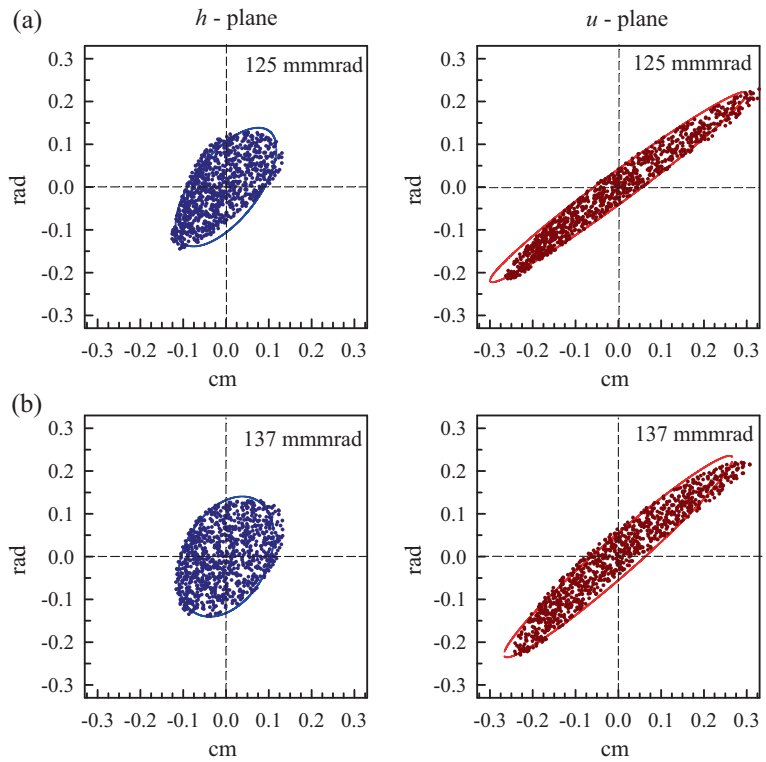

Figure 8. Phase-space ellipses in the h plane and u plane at the inflector effective exit: (**a**) represents the phase ellipses for a hard edge electric field and (**b**) represents the phase ellipses for RELAX3D field with reduced potential. Input beam parameters are $U(0) = H(0) = 2$ mm, $P_u(0) = P_h(0) = 0$ mrad and $\varepsilon_u(0) = \varepsilon_h(0) = 80$ mm mrad for both the cases at s_0.

where superscript C refers to the canonical variable. The transfer matrix so developed can be used to study the beam properties in the spiral inflector. To obtain the beam envelope sizes and emittances at the exit of the inflector, we need to calculate the six-dimensional beam matrix $\boldsymbol{\sigma}$ defined by

$$\boldsymbol{\sigma} = \langle \mathbf{x}\mathbf{x}^{\mathrm{T}} \rangle, \tag{13}$$

where $\langle\ \rangle$ denotes the average over the beam distribution. The evolution of the sigma matrix at position s can be obtained from the equation

$$\boldsymbol{\sigma}(s) = \mathbf{M}(s, s_0)\boldsymbol{\sigma}(s_0)\mathbf{M}^{\mathrm{T}}(s, s_0), \tag{14}$$

where $\boldsymbol{\sigma}(s_0)$ is the beam matrix at location s_0. The beam sizes and the emittances in the u and h planes at point s can be obtained from the following relations:

$$\begin{aligned} U(s) &= \sqrt{\sigma_{11}(s)}, \quad H(s) = \sqrt{\sigma_{33}(s)}, \\ \varepsilon_u(s) &= \sqrt{(\sigma_{11}\sigma_{22} - \sigma_{12}\sigma_{21})}, \\ \varepsilon_h(s) &= \sqrt{(\sigma_{33}\sigma_{44} - \sigma_{34}\sigma_{43})}. \end{aligned} \tag{15}$$

The procedure discussed was then used to study the behaviour of the projected emittances in both the transverse planes at the inflector exit for a hard edge electric field and a RELAX3D field with a reduced potential V_{inf}. The results are presented in figure 8. In the case of a hard edge field, the effect of the electric fringe field on the energy of the paraxial ion is taken by using the entrance and the exit kick options in the CASINO code. It is to be noted here that for the RELAX3D electric field, the entrance and exit of the infector are not at the start or end of the actual electrodes. The effective entrance of the infector is defined at a distance d_0 before the actual electrodes start and the effective exit is defined at a distance d_0 (5 mm) away from the actual end of the electrodes (see figure 6). In the present calculation, for both the cases, we have chosen the initial location ($s_0 = 0$ cm) sufficiently away from the actual electrode start and the exit location is at the effective exit of the inflector ($s = 4.4$ cm). The effective entrance of the inflector, actual electrode start and end locations are shown in figure 6.

The typical value of 90% normalised emittance of the oxygen beam from high charge state ECR ion sources varies between 0.1 and 0.2 mm mrad [28] which corresponds to the total emittance of 44 and 88 mm mrad, respectively, for O^{6+} ion at 6.41 kV extraction voltage. In the present paper, to some extent, we have taken the value of the emittances in this range. Figure 8 shows the orientations of phase ellipses at the effective exit of the spiral inflector ($s = 4.4$ cm) for an axisymmetric input beam at s_0 with $U(0) = H(0) = 2$ mm,

$P_u(0) = P_h(0) = 0$ mrad and equal uncoupled emittances $\varepsilon_u(0) = \varepsilon_h(0) = 80$ mm mrad. Solid curves represent the projected emittances in both the transverse planes obtained by using the transfer matrix method. Here the transfer matrix **M** is obtained by running CASINO as stated above and the beam parameters are obtained by using eqs (14) and (15). In each case, we have verified the symplectic condition imposed on the transfer matrix **M**. It is found that for both the cases, the magnitude of the projected emittances in both the planes is equal to each other at the exit of the inflector. There is also a substantial growth in the magnitude of the projected emittances at the exit of the inflector in both the planes due to the interplane coupling effects. This effect produces a diverging beam in the u plane. The estimated values of the projected emittances are 125 and 137 mm mrad for the hard edge field and the RELAX3D field respectively. We point out here that despite the growth of the projected beam emittances calculated in the u and h planes, there exists an invariant generalised emittance [17,29] for this coupled system which is given by $\varepsilon_{4d} = |\boldsymbol{\sigma}|^{1/4}$. This emittance always remains constant in the presence of plane coupling as long as the applied forces are linear. In the present case, the estimated value of the generalised emittance is $\varepsilon_{4d} = 80$ mm mrad which remains constant throughout.

To check the validity of the matrix approach in the present case, we have tracked 2000 representative particles through the spiral inflector that are distributed uniformly within $U(0) = H(0) = 2$ mm, $P_u(0) = P_h(0) = 0$ mrad and $\varepsilon_u(0) = \varepsilon_h(0) = 80$ mm mrad at s_0. The two-dimensional projections at the effective inflector exit in the u plane and h plane for both hard edge fields and RELAX3D field are shown in figures 8a and 8b, respectively, by dotted curves. It is easy to see from figure 8 that the number of tracked ions falling within the solid ellipse obtained by the sigma matrix method is slightly less in both cases. This occurs because the particles populated on the boundary of the phase ellipses encounter nonlinearities in the inflector field that cannot be taken into account by the inflector transfer matrix. These particles tend to appear beyond the phase-space boundary obtained by the linear matrix method.

To estimate beam sizes in the spiral inflector, the paraxial ion trajectories of 100 representative particles belonging to the boundary of the input emittances of 80 mm mrad with $U(0) = H(0) = 2$ mm, $P_u(0) = P_h(0) = 0$ mrad in each plane were run through the inflector. The resulting paraxial ion trajectories in the u and h planes within the inflector electrode are shown by solid lines in figure 9 for the RELAX3D field with reduced potential. The dashed lines indicate the electrode apertures. Here we have used $s_{\text{in}} = 0$ cm and $s_{\text{out}} = 4.4$ cm so that the entry of the electrode is at

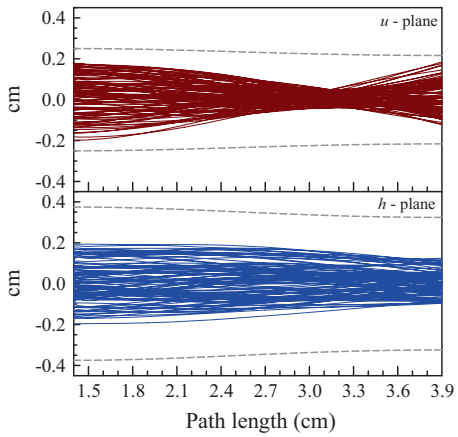

Figure 9. Paraxial ion trajectories through the spiral inflector in both the u and h planes for the RELAX3D electric field with reduced potential V_{inf}. Dashed lines represent the available electrode aperture.

$s = 1.4$ cm and the exit is at $s = 3.9$ cm (see figure 6). It is evident from figure 9 that the beam has a divergent characteristic in the u plane and converging behaviour in the h plane. As the available electrode aperture in the u plane is less than that in the h plane, we expect more beam loss in the u plane due to the restricted aperture. A careful optimisation of the injected beam at the input of the inflector is thus necessary to reduce the emittance growth at its exit and to keep beam sizes within a reasonable limit in both the planes.

4. Minimising transverse beam loss

In this section we discuss the transverse beam matching in the four-dimensional subspace (x, p_x, y, p_y) to minimise beam losses at the central region of the cyclotron by using system parameters of the existing axial injection line of K130 cyclotron. The axial injection system consists of 14.4 GHz ECR ion source producing a variety of light–heavy ion beams such as $O^{4+,5+,6+}$, $Ne^{5+,6+}$, $Ar^{8+,9+}$, etc. and an almost 8.2 m long beam transport line. The horizontal section of the transport line consists of an ion source, a solenoid magnet and a bending magnet that is used to bend as well as analyse the beam. The vertical section consists of three solenoids outside the cyclotron yoke and one inside the yoke. The last solenoid is a short solenoid with an x–y steerer magnet inside to match the position and the angle of the trajectories in the inflector. Finally, the beam will be injected into the central region of the cyclotron by a spiral inflector.

Injection from an external ion source into a cyclotron results in unavoidable emittance growth as the beam passes through the spiral inflector and varying axial magnetic field of the cyclotron. In this case, the two

transverse directions are coupled on entering the axial magnetic field of the cyclotron and the transverse and longitudinal phase spaces are coupled by the spiral inflector. Therefore, a careful optimisation of the beam line parameters is necessary to reduce transmission loss in the inflector and further acceleration into the cyclotron.

Optimisations are performed using the computer code TRANSOPTR [30,31] that is based on the $\boldsymbol{\sigma}$ matrix formalism. Here, the beam transport system is specified by a user supplied FORTRAN subroutine and there is more flexibility for imposing the fitting constraints and variable parameters. It uses the infinitesimal transfer matrix approach that allows the treatment of optical elements, such as varying axial magnetic field and a spiral inflector, where it is not possible to write down an analytic transfer matrix. TRANSOPTR employs the infinitesimal transfer matrix approach [32,33] in which the infinitesimal transfer matrix $\mathbf{F}(s)$ can be defined as $(\mathbf{T}-\mathbf{I})/\mathrm{d}s$, where s is the path length along the transport line, $\mathbf{T}$ is the transfer matrix from s to $s+\mathrm{d}s$ and $\mathbf{I}$ is the identity matrix. For single particle motion, we have

$$\mathbf{x}_{\mathrm{p}}'(s) = \mathbf{F}(s)\mathbf{x}_{\mathrm{p}}(s), \tag{16}$$

where $\mathbf{x}_{\mathrm{p}}(s) = (x, p_x, y, p_y)^{\mathrm{T}}$ represents the coordinates of a paraxial ray at location s. The relationship between optical (u, h, v) and the Cartesian (x, y, z) coordinate system is illustrated in figure 1 and is taken care of in these calculations. The beam matrix $\boldsymbol{\sigma}$ obeys the envelope equation [34]

$$\boldsymbol{\sigma}'(s) = \mathbf{F}(s)\boldsymbol{\sigma}(s) + \boldsymbol{\sigma}(s)\mathbf{F}^{\mathrm{T}}(s). \tag{17}$$

The $\mathbf{F}$ matrix of the usual beam line elements (solenoids, bending magnet, etc.) can be derived from the well-known equations of motion. The varying axial magnetic field and spiral inflector have been incorporated into TRANSOPTR using the $\mathbf{F}$ matrix given in detail in ref. [27]. Although a hard-edge approximation with an entrance and exit kick is assumed here in deriving the $\mathbf{F}$ matrix for the spiral inflector, it is adequate to perform the initial injection line optimisation before a more detailed analysis is taken up using a large number of particles with a realistic field.

We assumed the cyclotron as a dipole with a field index n nearly equal to 0.09 and produced an upright acceptance ellipse. The radial tune of the dipole field is $\upsilon_x = \sqrt{1-n} = 0.954$ and the corresponding vertical betatron tune is equal to 0.3. These values are very close to the tune values of the K130 cyclotron in the central region. The idea is to minimise the circulating emittances [35] in the cyclotron defined as $\varepsilon_x = \upsilon_x x_{\max}^2/R_{\mathrm{cy}}$, where R_{cy} is the radius of the cyclotron and $x_{\max}$ is the maximum beam size over one betatron oscillation. A similar equation is also valid in the y direction. Here, the circulating emittance is the area/π of the ellipse that is similar to the acceptance ellipse and that encloses the beam ellipse. We see that it can be minimised in each plane by minimising the maximum displacement over one betatron oscillation. This minimisation is performed using a simulated annealing algorithm in-built in TRANSOPTR. Matching is achieved by varying the strength of the solenoid magnets placed in the axial injection line by minimising the horizontal beam size at a location in the cyclotron separated by $90^\circ/\upsilon_x$ of the azimuth, and vertical beam size at a location separated by $90^\circ/\upsilon_z$.

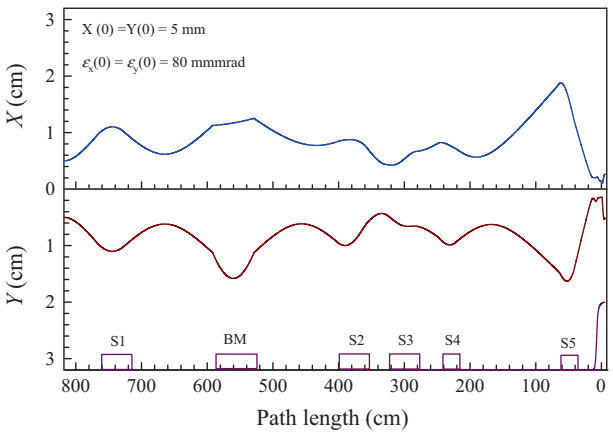

Figure 10. Optimised beam envelopes along the x and y directions for the input beam with $X(0) = Y(0) = 5$ mm, $P_x(0) = P_y(0) = 0$ mrad and equal emittance $\varepsilon_x(0) = \varepsilon_y(0) = 80$ mm mrad. The relation between the Cartesian (x, y, z) and optical (u, h, v) coordinated system in the spiral inflector is explained in figure 1.

The simulation results of the transverse matching of the O^{6+} ion beam having an injection energy of 38.45 keV to the central region of the cyclotron are plotted in figure 10. The initial beam is taken to be axisymmetric with $X(0) = Y(0) = 5$ mm, $P_x(0) = P_y(0) = 0$ mrad and equal emittance $\varepsilon_x(0) = \varepsilon_y(0) = 80$ mm mrad. The resulting beam envelopes producing a beam of unequal sizes in the x and y directions are shown by the blue and red solid lines, respectively. The first solenoid (S1) is used for focussing the beam to a waist near the object point of the vertical bending magnet whereas the last four solenoids (S2, S3, S4 and S5) are used for matching in the cyclotron. The location of the bending magnet, solenoid magnets and the varying axial magnetic field in the arbitrary scale are also shown in the plot. The optimised parameters of the beam line components are listed in table 3. It is easy to see from figure 10 that there is a rapid growth of the vertical beam size after the inflector exit. This is due to the lower value of the vertical betatron tune. The estimated vertical beam size in the first turn is about 4.5 mm which is well

Table 3. Parameters of the elements of the axial injection system for O^{6+}.

Element	Parameters	Values
Solenoid 1 (S1)	Length	43.6 cm
	Field	0.897 kG
Vertical bending magnet (BM)	Entry/exit angle	30.19°
	Bending angle	90°
	Bending radius	40 cm
Solenoid 2 (S2)	Length	43.6 cm
	Field	1.03 kG
Solenoid 3 (S3)	Length	43.6 cm
	Field	1.08 kG
Solenoid 4 (S4)	Length	26.7 cm
	Field	1.1 kG
Solenoid 5 (S5)	Length	21.7 cm
	Field	1.53 kG

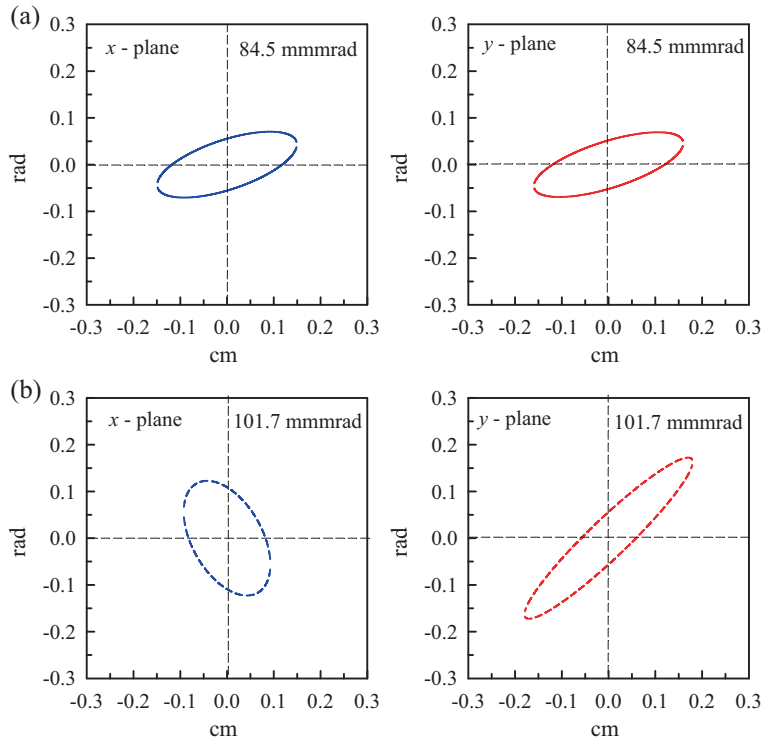

Figure 11. The phase ellipses at the (**a**) inflector electrode entrance and (**b**) matching point for the optimised values of the injection line parameters. The matching point is at $x = -0.39$ cm and $y = 1.75$ cm in the median plane.

within the available vertical aperture in the central region limited by the height of the Dee and Dummy Dee inserts from the median plane.

Figure 11 shows the orientations of the optimised phase ellipses, in two transverse planes at the entrance and the resulting phase ellipses at the matching point in the central region for the optimised injection line parameters. It is found from simulation results that the beam sizes in both the planes are well within the available electrode aperture in the spiral inflector. The estimated projected emittances in both the planes are 84.5 mm mrad at the inflector entrance. The optimised beam parameters at the matching point in the central region are $X(0) = 0.93$ mm, $P_x = -56$ mrad and $Y(0) = 1.8$ mm, $P_y = 163$ mrad with emittances $\varepsilon_x = \varepsilon_y = 101.7$ mm mrad which are reasonably less compared to the previous example (figure 8).

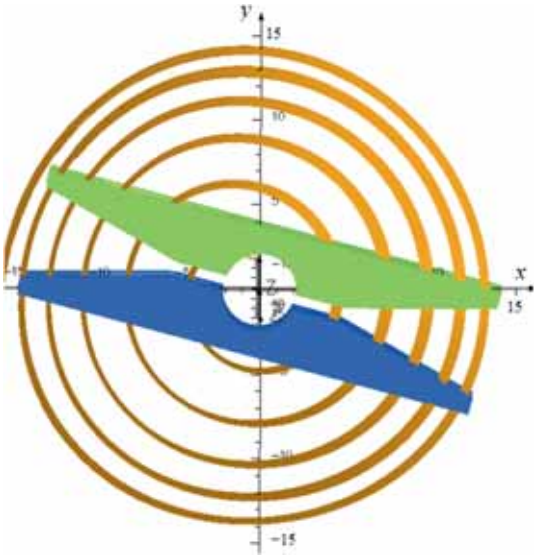

Figure 12. Trajectories of 500 particles for the first few turns in the central region with an optimised input condition at the matching point. Dee and Dummy Dee inserts are also shown. To make the trajectory visible, Dee (180°) and Dummy Dee are not plotted.

To see the behaviour of the particle trajectories in the central region of the cyclotron, numerical simulations are carried out for 500 particles that are within the optimised phase ellipses at the matching point (figure 11b). The particle tracking simulation has been performed using OPERA3D Post-Processor [23] which includes both computed electric and magnetic field data. Simulation results up to five turns are shown in figure 12 for O^{6+} ions with injection energy = 38.45 keV, Dee voltage = 48 kV, rf frequency = 6 MHz, harmonic number = 1 and initial phase = 110° with respect to rf. The maximal axial displacement of the trajectories is checked at each integration step. Those particles which are within the smallest vertical aperture of the central region survived. Figure 12 shows that most of the particles are well within the smallest vertical aperture of the central region except some particles (∼10%) lost on the inner surface of the Dee and Dummy Dee insert electrodes at the innermost radius. This result confirms that the optimised beam conditions match with the acceptance of the central region.

5. Conclusion

In this paper, we have discussed the design of a spiral inflector for inflecting heavy ions into the K130 variable energy cyclotron at Kolkata. It is found that the spiral inflector can be fitted into the space available in the central region without disturbing the configuration of the existing accelerating electrode. We have studied the effect of the fringe field on the optical properties of the beam of the spiral inflector and observed that it causes the central trajectories of the inflector to deviate from the design orbit. It is shown that to compensate this fringe field effect, a decrease of 7.8% of the bias electrode voltage is required. We have also studied the beam dynamics through the spiral inflector for the analytical hard edge field and the RELAX3D field by using the linear transfer matrix technique. We have not considered the effect of space charge in the analysis as the operating beam current in VEC is very low. It is found that the beam is more diverging in the vertical direction at the median plane and there is a substantial growth in the magnitude of the projected emittances due to the interplane coupling effects. We have optimised the injection line parameters to avoid transmission loss in the spiral inflector and to minimise beam losses in the central region of the cyclotron. We have also carried out particle tracking in the computed electric and magnetic fields in the central region with optimised phase ellipses at the matching point. It is observed that maximum particles are well within the smallest vertical aperture of the central region, validating the fact that the optimised beam conditions match with the acceptance of the central region.

Acknowledgements

The authors would like to express their sincere gratitude to Shri Amitava Roy and Dr Arup Bandyopadhyay of VECC, for their encouragement and support to this work. The authors would also like to thank Shri P S Chakraborty, Dr P Y Nabhiraj, Shri Suvadeep Roy and Shri C Nandi for providing information on the K130 cyclotron and its injection line.

References

[1] S Bhattacharya, S Mukhopadhyay, D Pandit, S Pal, A De, S Bhattacharya, C Bhattacharya, K Banerjee, S Kundu, T K Rana, A Dey, G Mukherjee, T Ghosh, D Gupta and S R Banerjee, *Phys. Rev. C* **77**, 024318 (2008)
[2] S Kundu, C Bhattacharya, S Bhattacharya, T K Rana, K Banerjee, S Muhkopadhayay, D Gupta, A Dey and R Saha, *Phys. Rev. C* **87**, 024602 (2013)
[3] P Sen, S K Bandyopadhyay, P M G Nambissan, P Barat and P Mukherjee, *Phys. Lett. A* **302**, 330 (2002)
[4] P Mukherjee, A Sarkar and P Barat, *Mater. Charact.* **55**, 412 (2005)
[5] A S Divatia and A Ambasankaran, *Pramana – J. Phys.* **24**, 227 (1985)
[6] S Chatterjee *et al*, *Proceedings of the 9th International Conference on Cyclotrons and their Applications* (Caen, France, 1981) p. 75

[7] A Jain, R C Sethi and A S Divatia, *Proceedings of the* 9*th International Conference on Cyclotrons and their Applications* (Caen, France, 1981) p. 69
[8] W B Powell and B L Reece, *Nucl. Instrum. Methods* **32**, 325 (1965)
[9] N Hazewindus, *Nucl. Instrum. Methods* **129**, 325 (1975)
[10] G Bellomo, D Johnson, F Marti and F G Resmini, *Nucl. Instrum. Methods* **206**, 19 (1983)
[11] L Belmont and J L Pabot, *IEEE Trans. Nucl. Sci.* **NS-13**, 191 (1966)
[12] L W Root, *Experimental and theoretical studies of the behavior of an H-ion beam during injection and acceleration in the TRIUMF central region model cyclotron*, Ph.D. thesis (University of British Columbia, Vancouver, 1974)
[13] D Toprek, *Nucl. Instrum. Methods A* **440**, 285 (2000)
[14] D Toprek, D Reistad, B Lundstrom and D Wessman, *Nucl. Instrum. Methods A* **486**, 539 (2002)
[15] V S Pandit, *Pramana – J. Phys.* **59**, 1019 (2002)
[16] R J Balden, W Kleeven, L S Milinkovic, B F Milton and J B Pearson, *Proceeding of the* 12*th International Conference on Cyclotrons and their Applications* (Berlin, Germany, 1989) p. 435
[17] A Goswami, P Sing Babu and V S Pandit, *Nucl. Instrum. Methods A* **693**, 276 (2012)
[18] A Goswami, P Sing Babu and V S Pandit, *Eur. Phys. J. Plus* **127**, 79 (2012)
[19] L W Root, *Design of an inflector for TRIUMF cyclotron*, M.Sc. thesis (University of British Columbia, Vancouver, 1972)
[20] M V Lachinov, *Design studies on the axial injection system of the CYCLONE*-44 *cyclotron*, Ph.D. thesis (University of British Columbia, Vancouver, 1998)
[21] C J Kost and F W Jones, *RELAX*3*D User's Guide and Reference Manual*, TRI-CD-88-01 (Vancouver, 1988)
[22] J H Kim, D H Lee and K S Chun, *J. Kor. Phys. Soc.* **46**, 1102 (2005)
[23] OPERA 15R2, Cobham Technical Services
[24] F B Milton and J B Pearson, *CASINO user's guide and reference manual*, TRI-DN-89-19 (Vancouver, 1989)
[25] L M Milinkovic, *RELAX*3*D spiral inflectors*, TR30-DN-89-21 (Vancouver, 1989)
[26] D Toprek, *Nucl. Instrum. Methods A* **449**, 435 (2000)
[27] R Baartman and W Kleeven, *Part. Accel.* **41**, 41 (1993)
[28] M Schlapp *et al*, *Rev. Sci. Instrum.* **69**, 631 (1998)
[29] A Goswami, P Sing Babu and V S Pandit, *Phys. Plasmas* **19**, 123105 (2012)
[30] M S de Jong and E A Heighway, *IEEE Trans. Nucl. Sci.* **NS-30**, 2666 (1983)
[31] E A Heighway and R M Hutcheon, *Nucl. Instrum. Methods* **187**, 89 (1981)
[32] F J Sacherer, *IEEE Trans. Nucl. Sci.* **NS-18**, 1105 (1971)
[33] F J Sacherer, *Transverse space-charge effects in circular accelerators*, Ph.D. thesis (University of California, Berkeley, 1968)
[34] W Kleeven and R Baartman, *Part. Accel.* **41**, 55 (1993)
[35] M Dehnel and K Erdman, *Proceeding of the* 4*th European Particle Accelerator Conference* (London, 1994) p. 2367